Supplementary information

Solvent effect in the chemical design of coordination polymers of various topologies with Co^{2+} and Ni^{2+} ions and 2-furoate anions

Uvarova, Marina (contact); Lutsenko, Irina; Babeshkin, Konstantin; Efimov, Nikolay; Shmelev, Maxim; Alexandrov, Eugeny; Sokolov, Andrey; Eremenko, Igor; Khoroshilov, Andrey; Kiskin, Mikhail

N.S. Kurnakov Institute of General and Inorganic Chemistry of the Russian Academy of Sciences, Leninsky Prosp. 31, 119991 GSP-1, Moscow, Russian Federation
Fax (495) 952 1279. E-mail: yak_marin@mail.ru
[b] *Moscow Institute of Physics and Technology, 9 Institutskiy per, Dolgoprudny, Moscow Region, 141701, Russian Federation*
[c] *Samara State Medical University, Chapaevskaya st., Samara, Russian Federation, 443099*

Magnetic properties of 1-4

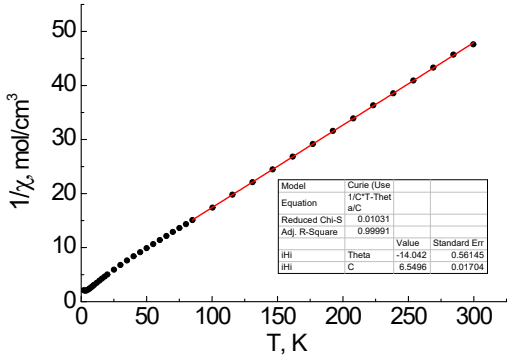

Figure 1S. Temperature dependence of 1/χ for compound **1** measured at H_{DC} = 5000 Oe. Red line represents fit using Curie-Weiss equation.

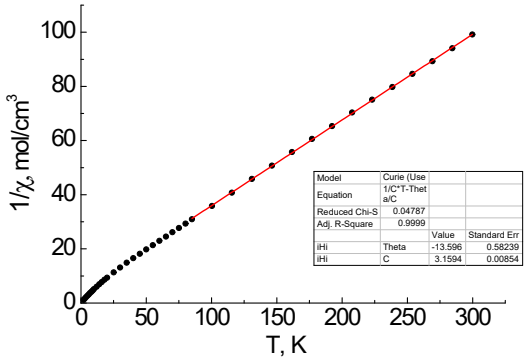

Figure 2S. Temperature dependence of 1/χ for compound **2** measured at H_{DC} = 5000 Oe. Red line represents fit using Curie-Weiss equation.

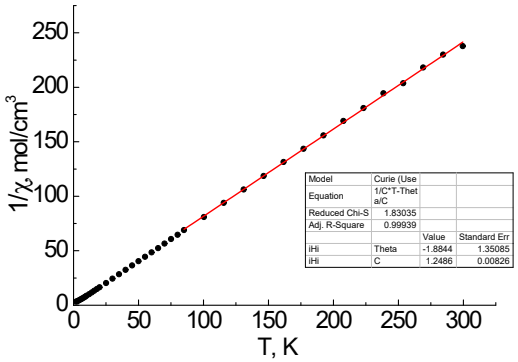

Figure 3S. Temperature dependence of 1/χ for compound **3** measured at H_{DC} = 5000 Oe. Red line represents fit using Curie-Weiss equation.

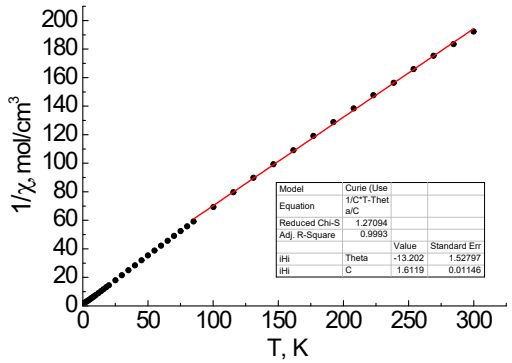

Figure 4S. Temperature dependence of 1/χ for compound **4** measured at H_{DC} = 5000 Oe. Red line represents fit using Curie-Weiss equation.

Table 1S. Fitting parameters using Curie-Weiss equation.

Complex	Θ	C
1	-14.0	6.55
2	-13.6	3.16
3	-1.9	1.25
4	-13.2	1.61

Magnetic properties in the ac-magnetic field.

In order to find out whether compounds **1-4** formed by Co^{2+} and Ni^{2+} exhibit slow relaxation of magnetization, their magnetic dynamic was probed by measuring the ac-magnetic susceptibility. For complexes **1**, **3** and **4** no slow relaxation of magnetization was observed under any magnetic fields and at any temperature. The values of χ'' were unsignificant in comparison with the χ' values. For complex **2**, however, quite complicated magnetization relaxation dynamic was obtained.

In the zero dc-magnetic field, the out-of-phase values are negligible at 2 K for ac-frequencies in the range from 10 to 10000 Hz (Figure 8S). The absence of considerable $\chi''(\nu)$ signals for complex **2** likely originates from significant contribution from the quantum tunneling of the magnetization (QTM) resulting in fast relaxation. For minimizing the effect of QTM, non-zero dc-fields up to 5000 Oe have been applied. This resulted in appearance of the significant out-of-phase signals on the $\chi''(\nu)$ dependencies. Based on this data the optimal value of the dc-field strength (at which the relaxation speed is the smallest) was selected as 1000 Oe (Figure 8S). Frequency dependences of the in-phase and out-of-phase components of the ac-magnetic susceptibility for complex **2** taken under 1000 Oe field shown on Figure 9S.

The corresponding $\chi''(\nu)$ isotherms were approximated by use the generalized Debye model. This yielding temperature dependences of relaxation time (τ vs. 1/T) shown on Figure 10S. Overall non-linear course of these dependences evidences contribution of non-Orbach magnetization relaxation mechanisms in both the cases. On the obtained τ vs. 1/T graph one can observe two unresolved peaks. This effect may appear due to disorder of the H^+ ion in a molecule coordinated to the magnetic center.

For complex **2** in the high-temperature range the $\tau(1/T)$ dependences were approximated by Arrhenius equation ($\tau = \tau_0 \cdot \exp(\Delta_{eff}/kT)$) for slower relaxation process 5.5-7.5 K, faster relaxation process 4-5.5 K. Such an approximation affords following sets of relaxation parameters: Δ_{eff}/k_B = 51 K, $\tau_0 = 1\times10^{-8}$ s for slow relaxation and Δ_{eff}/k_B = 17 K, $\tau_0 = 1.2\times10^{-6}$ s for faster relaxation process. The best fits of the entire τ *vs.* 1/T dependence for **2** were achieved by involving sum of Orbach and Raman ($\tau^{-1} = C_{Raman}T^{nRaman}$) with parameters Δ_{eff}/k_B = 45, $\tau_0 = 3.0\times10^{-8}$ s, C_{Raman}= 17 $s^{-1}K^{-nRaman}$, n_{Raman} = 2.7 with R^2= 0.9991 for slower relaxation process. For faster relaxation process Raman and direct ($\tau^{-1} = A_{direct}H^4T$) relaxation mechanisms were used with following parameters: C_{Raman}= 0.004 $s^{-1}K^{-nRaman}$, n_{Raman} = 9, $A_{direct} = 3.5\times10^{-9}$ $K^{-1}Oe^{-4}s^{-1}$ with R^2= 0.95901.

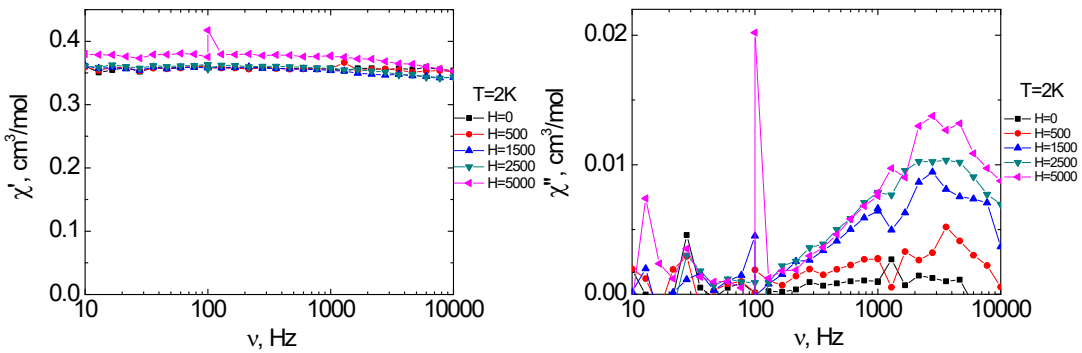

Figure 5S. Frequency dependences of the real (χ', left) and imaginary (χ'', right) components of the ac susceptibility under at 2 K for **1** in various dc-fields. Solid lines are visual guides.

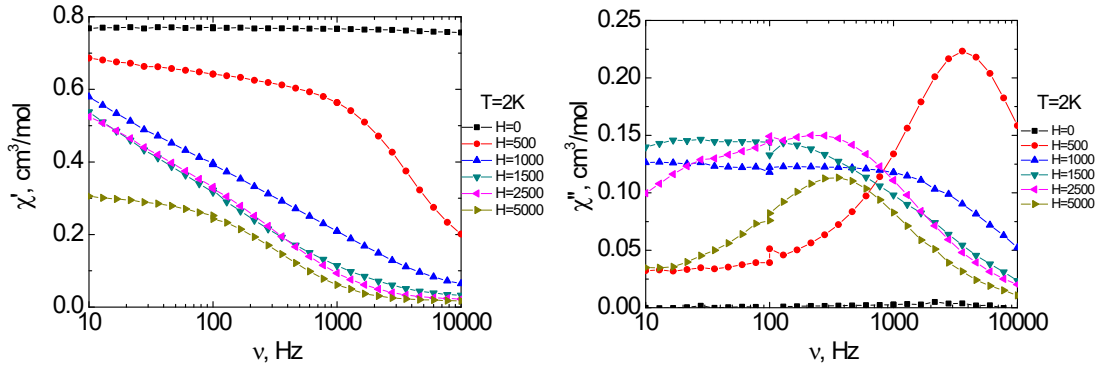

Figure 6S. Frequency dependences of the real (χ', left) and imaginary (χ'', right) components of the ac susceptibility under at 2 K for **2** in various dc-fields. Solid lines are visual guides.

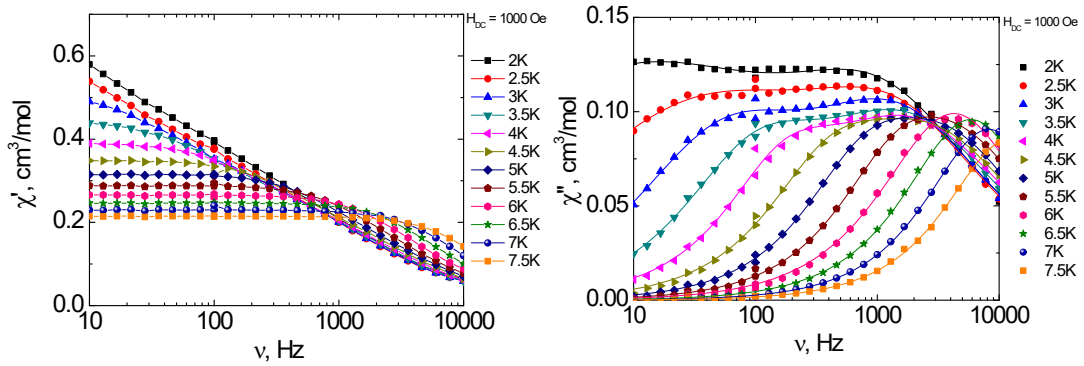

Figure 7S. Frequency dependences of the real (χ', left) and imaginary (χ'', right) components of the ac susceptibility under at 1000 Oe dc-field for **2** under various temperatures. Solid lines are visual guides (left), generalized Debye approximation (right).

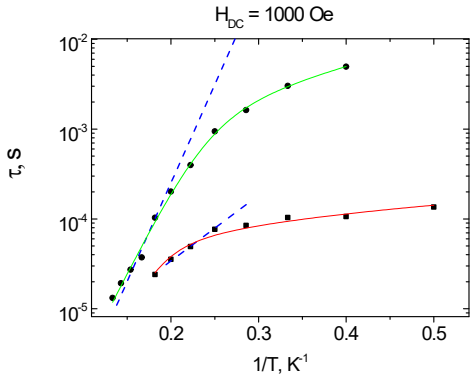

Figure 8S. – Dependence of the relaxation time τ on the reciprocal temperature for complex **2** in a magnetic field Hdc = 1000 Oe. The data was obtained by approximating the frequency dependences of the imaginary part of the dynamic magnetic susceptibility using the generalized Debye model. The blue dotted line is the approximation of high-temperature data by Arrhenius equation. The red line is the approximation by equation of the sum of Raman and direct relaxation mechanisms. The green line is the approximation by equation of the sum of Orbach and Raman relaxation mechanisms.

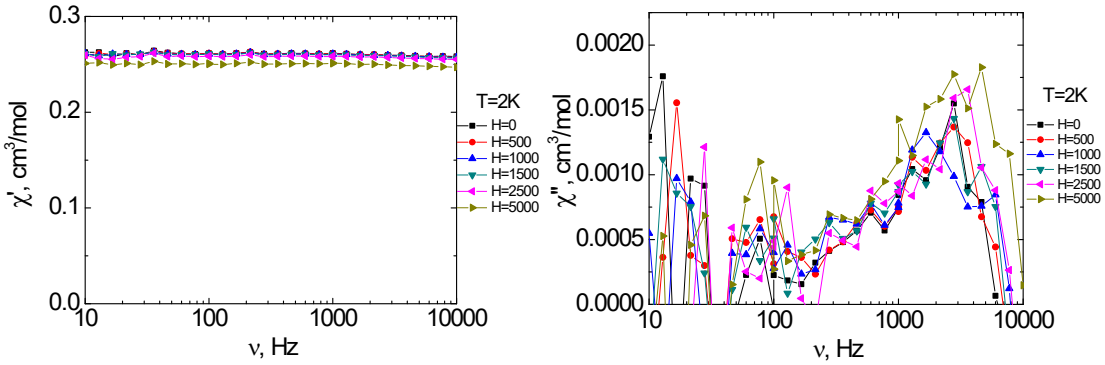

Figure 9S. Frequency dependences of the real (χ', left) and imaginary (χ'', right) components of the ac susceptibility under at 2 K for **3** in various dc-fields. Solid lines are visual guides.

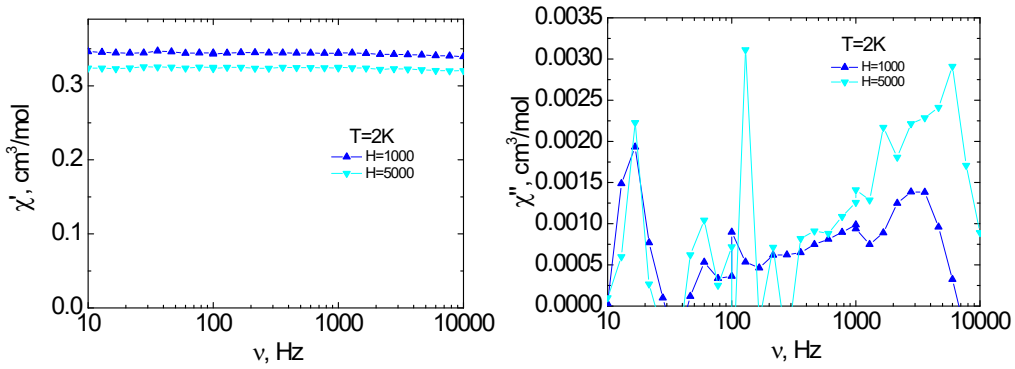

Figure 10S. Frequency dependences of the real (χ', left) and imaginary (χ'', right) components of the ac susceptibility under at 2 K for **4** in various dc-fields. Solid lines are visual guides.

\

Thermal properties 1, 3 and 4

Thermal behavior of **1**, **3** and **4** was studied by STA method under argon with simultaneous TG and DSC recording (Fig. 6 a,b). Complex **1** is the most stable in the series of coordination polymers studied and is not subject to changes up to 295 °C. Apparently, the linear organization of the supramolecular level (Fig. 1) in combination with the intramolecular hydrogen bonds causes the thermal stability effect. The first endothermic effect with an extremum at 329 °C corresponds to the release of the N-donor ligand and coordinated methanol molecules (Fig. 12S red; Table S2). The total mass loss at this stage is 22.2% ($m_{calc.}$ = 23.3%) (Fig. 12S blue; Table 2S). The final second stage (341-371 °C) is accompanied by the decomposition of the remaining organic part, which is not eliminated completely until the end of thermolysis (the final mass is considerably greater than the mass of the metal oxide that is formed most commonly upon thermal decomposition of carboxylate complexes .

In contrast to **1**, the first indications of mass loss in **3** and **4** are observed already at 50 and 84 °C, respectively (Fig. 12S, blue; Table 2S). An endothermic effect with an extremum at 113 °C that is observed only in the case of **4** (Fig. 12S, red) corresponds to the removal of external water molecules ($m_{calc./found}$ = 2.9% / 3.2%; the calculation was made for the monohydrate since storage of solvated systems is accompanied by naturally occurring physical desorption of solvent molecules).

Table 2S. Thermal analysis data for 1, 3 and 4 (inert atmosphere).

Complex	Stage / ΔT, °C	Δm (TG), %	T_{endo}, °C	$m_{fin,}$ %
1	1 (295–341)	22.2	329±0.7	
	2 (341–371)	51.8	365±0.7	26
3	1 (50–202)	3.1	-	
	2 (202–289)	23.1	261±0.7	
			279±0.7	
	3 (289–388)	56.8	381±0.7	17
4	1 (84–147)	3.4	113±0.7	
	2 (147–293)	12.6	261±0.7	
			279±0.7	
	3 (293–371)	61.0	381±0.7	23

The second and third steps for **3** and **4** generally lie in similar temperature ranges: the small endothermic effects at 261 °C (**3**) / 260 °C (**4**) (Fig. 12, red; Table 2S) correspond to the beginning of the thermal conversion of dpe molecules. In general, the final stage of thermolysis of compounds **1**, **3**, and **4** is characterized by powerful endothermic effects similar in form and intensity that correspond to the decomposition and subsequent desorption of the organic part of the complexes. A correlation between the extremums of the endo-effects and the structural organization of the complex is observed: 381 °C (3) > 365 °C (1) 357 °C (2). (Compound 3 contains no coordinated solvent molecules, whereas 4 contains not only coordinated but also outer-sphere water molecules that reduce the overall complex stability). The final products of thermolysis are carbonized metal oxides with various morphologies of the residues. (Fig. 13S).

The sample **4** is characterized by a three-dimensional framework containing pores filled with solvate water molecules according to data of single-crystal X-ray diffraction analysis. The calculated volume of these pores is 29.4% of the total cell volume (Fig. 3, 4). The presence of such pores in **4** suggests that the complex should have sorption properties provided that its framework is stable after dehydration. It was assumed that dehydration of **4** should be performed under relatively mild conditions (STA results (Fig. 12S) showed that **4** was stable up to 84 °C) not affecting the coordinated water molecules. Therefore, based on the results of STA, the samples were dehydrated at 30 and 60°C.

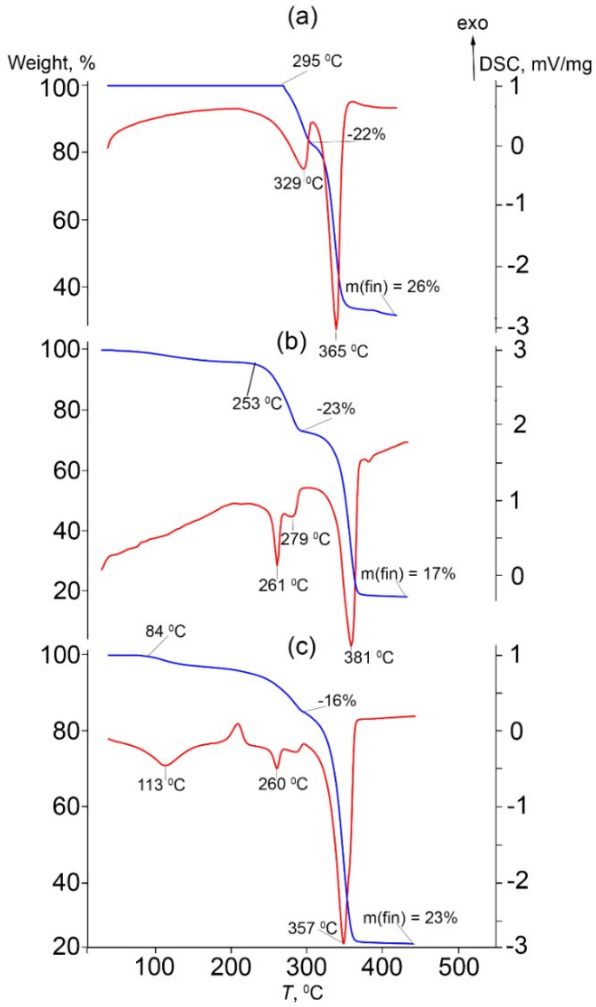

Figure. **11S**. TG (blue) and DSC (red) curves of 1 (a), 3 (b) and 4 (c).

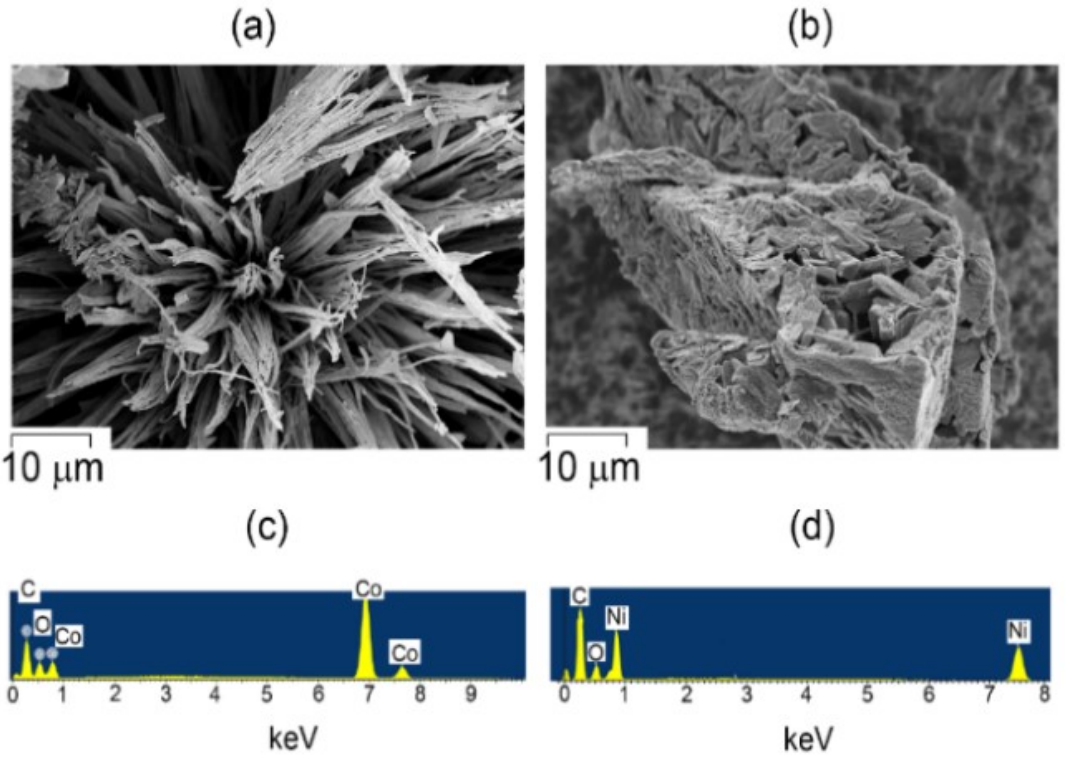

Figure **12S**. SEM microphotographs (a (1), b (3)) and EDX spectrum (c (1), d (3)) of the end-products (500 °C).

(a) (b)

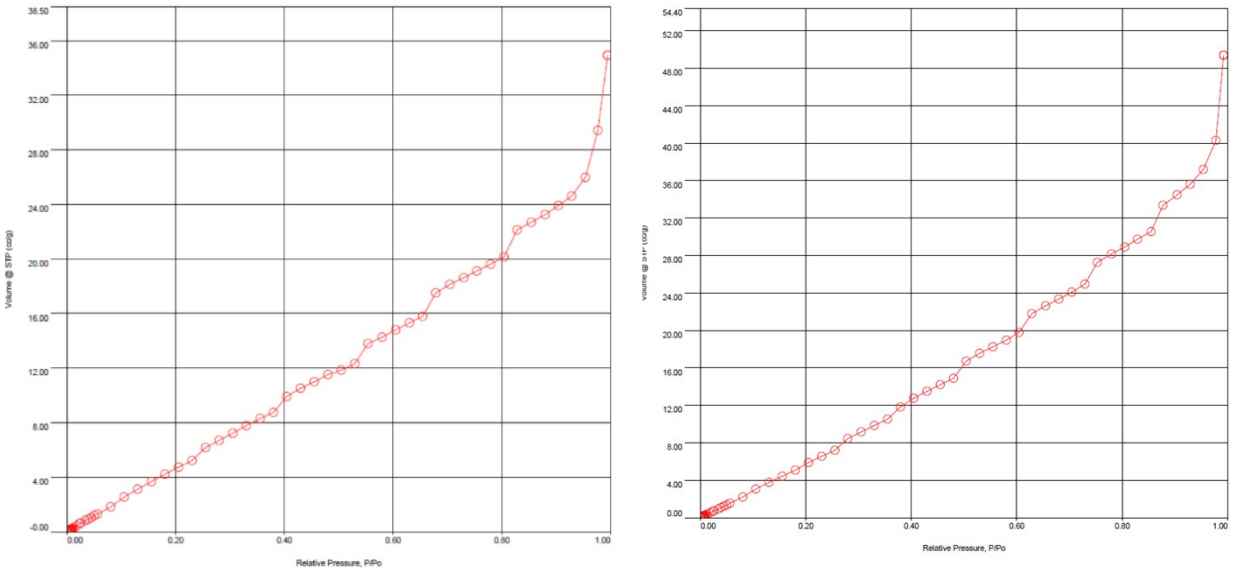

Figure 13S. Sorption isotherms (N_2) **4** after heat treatment at 30 °C (a) and 60 °C (b).

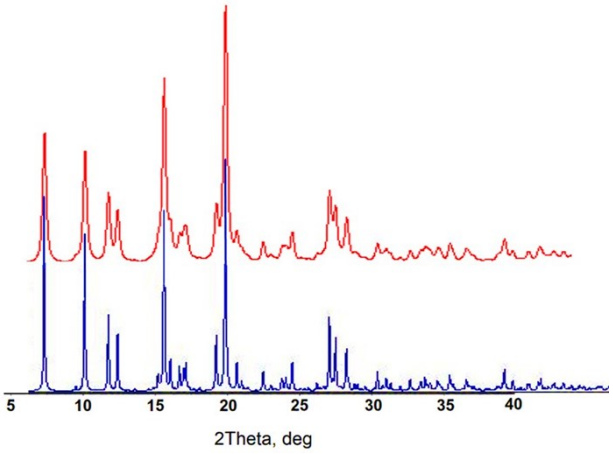

(b)

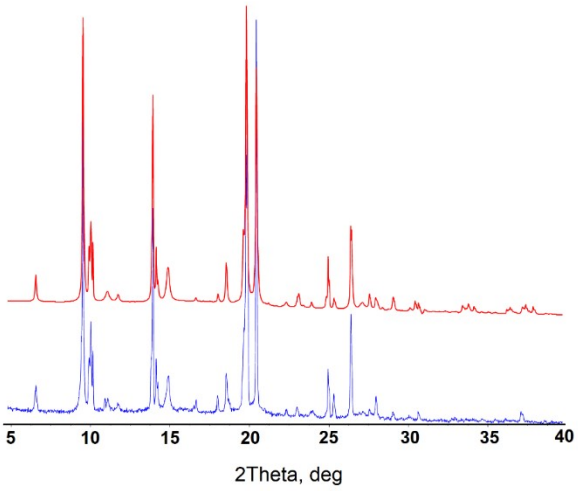

(c)

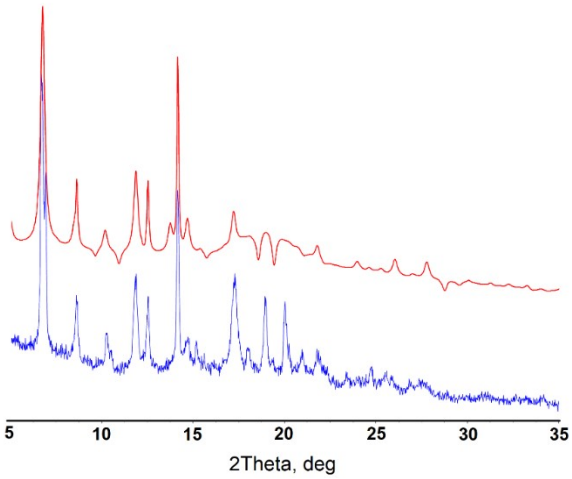

Figure 14S. PXRD patterns of **1 (a), 3 (b), 4 (c)** by the simulated from crystal data (red) and experimental (blue)